


Glycoproteins Hot Paper


Synthetic Homogeneous Glycoforms of the SARS-CoV-2 Spike Receptor-Binding Domain Reveals Different Binding Profiles of Monoclonal Antibodies

Farong Ye, Jie Zhao, Peng Xu, Xinliang Liu, Jing Yu, Wei Shangguan, Jiazhi Liu, Xiaosheng Luo, Cheng Li, Tianlei Ying, Jing Wang, Biao Yu, and Ping Wang*

Abstract: SARS-CoV-2 attaches to its host receptor, angiotensin-converting enzyme 2 (ACE2), via the receptor-binding domain (RBD) of the spike protein. The RBD glycoprotein is a critical target for the development of neutralizing antibodies and vaccines against SARS-CoV-2. However, the high heterogeneity of RBD glycoforms may lead to an incomplete neutralization effect and impact the immunogenic integrity of RBD-based vaccines. Investigating the role of different carbohydrate domains is of paramount importance. Unfortunately, there is no viable method for preparing RBD glycoproteins with structurally defined glycans. Herein we describe a highly efficient and scalable strategy for the preparation of six glycosylated RBDs bearing defined structure glycoforms at T323, N331, and N343. A combination of modern oligosaccharide, peptide synthesis and recombinant protein engineering provides a robust route to decipher carbohydrate structure-function relationships.

Introduction

The coronavirus SARS-CoV-2 pandemic has now infected more than 89 million people and caused over 1.9 million deaths around the world since December 2019. SARS-CoV-2, the key culprit pathogen of COVID-19^[1] that is similar to SARS-CoV-1, features the virus surface spike (S) glycoprotein which attaches the virus to the host cell receptor angiotensin-converting enzyme 2 (ACE2) via its receptor-binding domain (RBD).^[2] Given its key role in virus-host cell entry, the S protein and its RBD are primary targets for therapeutics and vaccine design (Figure 1B). In clinical settings, anti-RBD antibodies and vaccines based on the RBD as antigen have been recently employed against

How to cite: *Angew. Chem. Int. Ed.* **2021**, *60*, 12904–12910
International Edition: doi.org/10.1002/anie.202100543
German Edition: doi.org/10.1002/ange.202100543

COVID-19.^[3] The S protein of SARS-CoV-2 is heavily glycosylated, containing 22 N-linked glycosylation sites and several possible O-linked glycosylation sites (Figure 1A).^[4] The highly heterogeneous glycoforms of the S protein play important roles not only in modulating protein conformation and stability, but also in promoting immune evasion by shielding immunogenic epitopes from neutralizing antibodies, thereby impacting vaccine-induced immune responses.^[5] In line with the extensively glycosylated S protein, the RBD of the SARS-CoV-2 S protein contains two highly variable N-linked glycans (N331, N343) and two possible low-abundance O-linked glycans (T323, ca. 11 %; S325, 4 %, Figure 1B).^[4a,c] Notably, Watanabe and co-workers reported that 331 and 343 sites are dominated by complex-type N-glycans decorated with significantly high levels of fucosylation.^[4a] It is known that two glycosylation sites N331 and N343 are critical for viral infectivity. Removing N-glycosylation at N331 and N343 has been shown to decrease viral infectivity dramatically, highlighting the importance of glycans for the function of viral proteins.^[6] Importantly, interactions between N-glycans of RBD with different human lectins were recently reported by Ereño-Orbea and co-workers.^[7] Considering different pharmacodynamics and biological properties triggered by the microheterogeneity of various glycoforms, comprehending the precise correlations between glycan structures of each glycosylation site on the RBD and the structure related glycan functions is in high demand.

However, current gene expression systems lead to highly complex and heterogeneous RBD glycoforms, ranging from high-mannose variants to complex structures that are inseparable. To our knowledge, there are no studies of isolated or synthetic RBDs bearing homogeneous glycans for structure-

[*] F. Ye, J. Zhao, X. Liu, Dr. J. Liu, X. Luo, Prof. P. Wang
Shanghai Key Laboratory for Molecular Engineering of Chiral Drugs, School of Chemistry and Chemical Engineering, Frontiers Science Center for Transformative Molecules, Shanghai Jiao Tong University Shanghai 200240 (China)
E-mail: wangp1@sjtu.edu.cn

P. Xu, J. Yu, W. Shangguan, J. Wang, Prof. B. Yu
State Key Laboratory of Bioorganic and Natural Product Chemistry, Center for Excellence in Molecular Synthesis, Shanghai Institute of Organic Chemistry, Chinese Academy of Sciences
Shanghai 200032 (China)

C. Li, Prof. T. Ying
Laboratory of Medical Molecular Virology (MOE/NHC/CAMS), School of Basic Medical Sciences, Fudan University
Shanghai 200032 (China)

J. Wang
Institutes for Life Sciences, School of Medicine and National Engineering Research Center for Tissue Restoration and Reconstruction, South China University of Technology
Guangdong 510006 (China)

Prof. P. Wang
Key Laboratory of Systems Biomedicine (Ministry of Education), Shanghai Center for Systems Biomedicine
Shanghai Jiao Tong University, Shanghai 200240 (China)

 Supporting information and the ORCID identification number(s) for the author(s) of this article can be found under:
 <https://doi.org/10.1002/anie.202100543>.

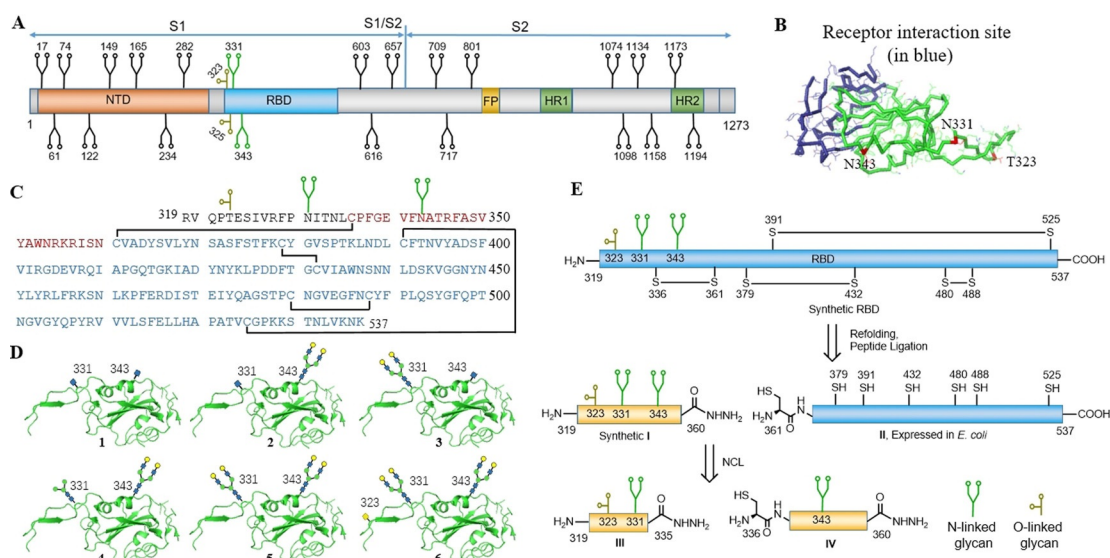


Figure 1. An overview of the SARS-CoV-2 Spike protein and its RBD. A) Representation of the glycosylated SARS-CoV-2 Spike protein structure. NTD, N-terminal domain; RBD, receptor binding domain; FP, fusion peptide; HR1, heptad repeat 1; HR2, heptad repeat 2. B) A structural model of glycosylated SARS-CoV-2 RBD, the colored red sites for T323, N331, and N343 glycosylation (PDB code: 6WPS). C) Homogeneous sequence of SARS-CoV-2 Spike RBD bearing two N-linked glycans (N331 and N343) and one O-linked glycan (T323) at the glycosylation sites, respectively (GenBank Accession: MN908947). D) Target RBDs (1–6) bearing homogeneous glycan at T323, N331 and N343. E) Retrosynthetic analysis of the homogeneous glycosylated RBD.

activity studies. Furthermore, beyond the well-defined nature, a defined glycosyl structure can be used as an epitope mimic and offers a route for rational immunogen design.^[8] For these reasons, we are interested in investigating the profiles of RBD glycans. We believe that chemical synthesis can offer homogeneous, complex RBD molecules for a detailed investigation of the specific roles of RBD glycoforms. In this context, we prepared RBDs containing homogeneous N-linked glycans at N331 and N343. In addition, considering the impact of O-glycan, an O-glycan at T323 was incorporated to explore its function. Despite recent rapid progress in oligosaccharide^[9] and protein synthesis,^[10] the size, physical properties, high structural diversity and complexity of RBD glycoproteins represent a significant synthetic challenge.^[11]

Structurally, the RBD (R319-K537) consists of a 5-stranded antiparallel β -sheet and four disulfide linkages, Cys336-Cys361, Cys379-Cys432, Cys391-Cys525, and Cys480-Cys488, which are formed to stabilize the core structure (Figure 1 C). No chemical synthesis route has been reported for homogenous RBD preparation. Herein we report an efficient semi-synthesis and structure–activity relationship (SAR) study of glycosylated RBDs (1–6) containing homogeneous N-linked glycans at N331, N343, and O-linked glycan at T323 (Figure 1 D). Evaluation of the Cys and glycosylation positions in the RBD structure suggests that expressed protein ligation (EPL)^[12] is an ideal strategy for the construction of glycosylated RBDs. Given the position of glycans and Cys residues, the retrosynthesis of the RBD was divided into two fragments: a synthetic glycopeptide RBD (319–360) fragment **I** with N/O-glycans, which was functionalized with a C-terminal hydrazide; and a recombinant RBD fragment **II** (361–537) possessing an N-terminal Cys residue facilitating native chemical ligation (NCL)^[13] (Figure 1 E). With these

two fragments in hand, the subsequent manipulation by EPL and refolding process provides the efficient synthesis of homogeneous glycosylated RBDs. In addition, to elucidate the functions of individual defined oligosaccharide structures, the glycopeptide domain (319–360) was further divided into two parts (R319-L335 **III** and C336-N360 **IV**) according to the position of glycans, with the presence of C336 acting as a handle for NCL. These preliminary results of structure–activity relationship (SAR) elucidate the structure–activity relationship between glycosylation and the viral infectivity. Furthermore, considering the highly conserved sequence of SARS-CoV-1/2 S protein RBD, we envision that this strategy will also serve as a versatile synthetic platform for homogeneous glycosylated RBDs of the SARS-CoV-1/2 S protein and other virus proteins.

Results and Discussion

Our synthesis started from the preparation of RBD fragment **II** (C361-K537), an expressed protein bearing an N-terminal Cys that is indispensable for subsequent native chemical ligation. This protein was expressed smoothly in *Escherichia coli*, and the initial methionine was efficiently cleaved simultaneously by endogenous methionine aminopeptidase. Next, protein fragments from inclusion bodies were solubilized in 6 M guanidine hydrochloride (GND-HCl) and purified via reverse phase HPLC followed by lyophilization. The desired product **II** was obtained as an amorphous white powder with a good yield of 30 mgL⁻¹ (see the Supporting Information, page 5 for details). Analysis by HPLC, HRMS and SDS-polyacrylamide gel electrophoresis

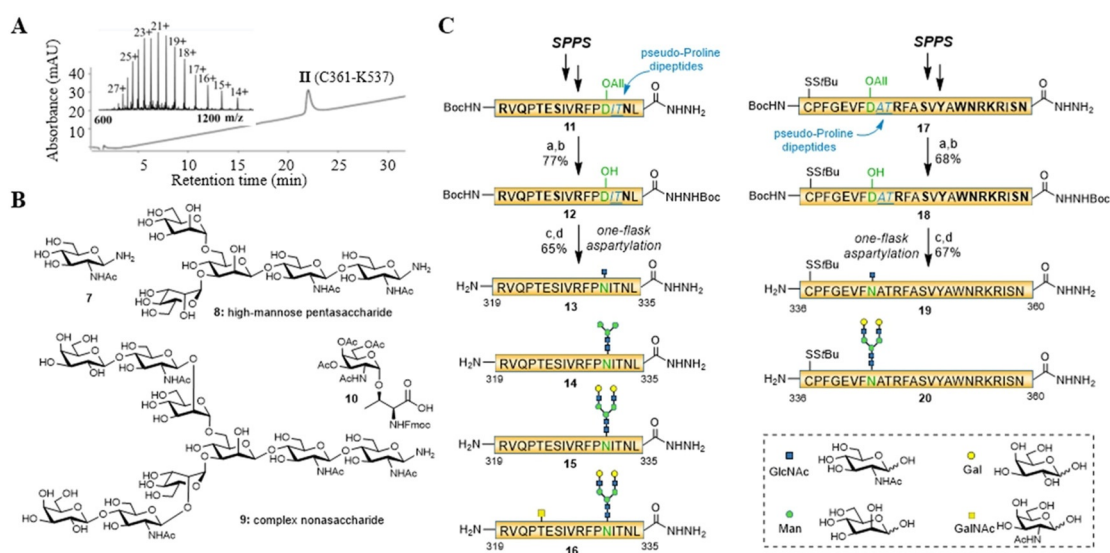


Figure 2. Preparation of RBD fragments II, III, and IV. A) Characterization of recombinant fragment II (C361-K537) using HPLC and HRMS. B) Chemical structure of glycosyl amines (7–9) and Thr glycosyl amino acids 10 used in the synthesis of glycopeptides. Monosaccharide 7, pentasaccharide 8 and nonasaccharide 9. C) Preparation RBD fragments III (13–16) and IV (19 and 20). Reaction conditions. a) Boc_2O , NaHCO_3 , THF; b) $\text{Pd}(\text{PPh}_3)_4$, PhSiH_3 , DCM (77% for 12, 68% for 18, over two steps); c) glycosyl amine, HATU, DIPEA, DMSO; d) Cocktail B (65% for 13, 61% for 14, 60% for 15, 67% for 19, 56% for 20 over two steps). Amino acids containing acid-labile protecting groups are shown in bold, pseudoproline dipeptides are shown in blue (underlined). Protecting groups are: R (Pbf), Q (Trt), E (tBu), S (tBu), N (Trt), Y (tBu), W (Boc), K (Boc), Y (tBu). Boc_2O , HATU, O-(7-azabenzotriazol-1-yl)-N,N,N',N'-tetramethyluronium hexafluorophosphate. DIPEA, diisopropylethylamine. DMSO, dimethylsulfoxide. TFA, trifluoroacetic acid. Pbf, 2,2,4,6,7-pentamethylidihydrobenzofuran-5-sulfonyl group.

(SDS-PAGE) confirmed the purity of the desired fragment II (Figure 2A and Figure 3F).

Regarding the oligosaccharide structure, we sought to install different glycoforms at N331 and N343, which could be used to probe the influence of N-linked glycans. In this event, we initially used less complex GlcNAc unit for N331 and N343 sites to explore the synthetic route. In a more complex setting, considering the major complex-type N-glycans at N331 and N343 sites, we elected to employ the complex-type nonasaccharide as N-glycan due to its accessibility.^[11b,f] Furthermore, it was reported that the N331 was composed of both complex and core type glycans.^[14] Therefore, the core pentasaccharide was utilized for N331 glycosylation. Thus, glycosyl amines 7 (GlcNAc), 8 (Man3GlcNAc2 pentasaccharide) and 9 (complex type, nonasaccharide) were prepared for aspartylation according to known methods (Figure 2B, see the Supporting Information, page 7 for details).^[11f,15]

The syntheses of these glycosylated peptides started from the preparation of the fully protected peptide 11, which was produced by Fmoc solid-phase peptide synthesis (SPPS) and Liu peptide hydrazide protocol.^[16] A pseudoproline group at the I332-T333 was used to suppress the possible aspartimide formation during Lansbury aspartylation (Figure 2C).^[15b,17] Then, hydrazide 11 was protected with a Boc group in the presence of Boc_2O , followed by selective palladium-mediated deallylation of D331, leading to peptide acid 12 smoothly at 77% yield over two steps. The employment of Boc-hydrazide was intended to avoid undesired amide bond formation between the free carboxylic acid 12 and glycosyl amine 7 during aspartylation. Next, HATU-assisted coupling of the carboxylic acid at D331 with glycosyl amine (7–9) under one-flask aspartylation/deprotection conditions, followed by

Cocktail B (TFA/ H_2O /*i*-Pr₃SiH/phenol, 88:5:2:5, v/v/v/v) deprotection and HPLC, generated three glycopeptides including 13 (GlcNAc), 14 (Man3GlcNAc2) and 15 (nonasaccharide) in good yields. Next, we induced GalNAc at T323 to probe the influence of O-linked glycan. It has been reported that the structure of the Tn-Thr antigen is important for molecular recognition due to its effect on peptide conformation.^[8d] An acetylated O-linked Thr glycosyl amino acid 10 was prepared following previous protocols and employed directly in Fmoc-SPPS.^[18] After one-flask aspartylation and subsequent deacetylation of O-glycan using 10% aqueous hydrazine, followed by single reversed-phase HPLC purification, the desired glycopeptide 16 was isolated at 52% yield over three steps. Thus, four glycopeptides III (fragments R319-L335, 13–16) were efficiently synthesized.

For the preparation of C336-N360 fragment IV, a similar protocol was applied to prepare desired glycopeptides. However, the preparation of peptide hydrazide-bearing C-terminal Asn was a challenge due to the cyclized imide formation between the hydrazide and side-chain amide of Asn during the TFA deprotection procedure.^[16] In this event, the SPPS synthesis produced fully protected peptide hydrazide 17 at 45% isolated yield after cleavage from the resin (see SI for details). A pseudoproline dipeptide at A344-T345 was readily incorporated to prevent the problematic aspartimide formation, the N-terminal Cys was protected by an S*t*Bu group (Figure 2C). After C-terminal protection of the peptide hydrazide 17 with a Boc group and palladium-assisted deallylation of D343, the peptide 18 with free aspartic acid was obtained successfully at 68% yield over two steps. Following the one-flask aspartylation/deprotection protocol, the resulting carboxylic acid was coupled with glycosyl amine

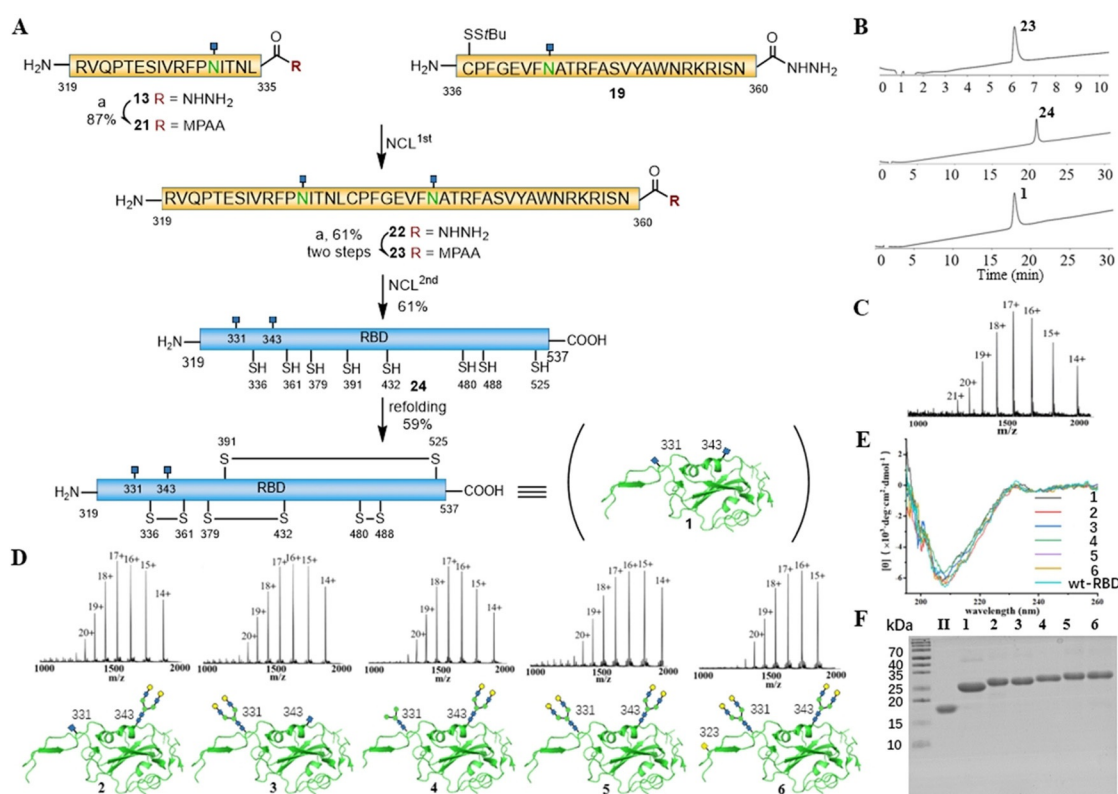


Figure 3. Preparation and characterization of glycosylated RBDs bearing various homogeneous glycoforms. A) Ligation and refolding protocol for glycosylated RBD 1. Reaction conditions: a) peptide hydrazide activation, 6 M GND-HCl, 0.2 M Na₂HPO₄, 0.1 M MPAA, 1.1 equiv acetylacetone (acac), pH 7.2, 37 °C, 4 h. NCL^{1st}: 6 M GND-HCl, 200 mM Na₂HPO₄, 50 mM TCEP, 100 mM MPAA, pH 6.8, 25 °C, 2 h. NCL^{2nd}: 6 M GND-HCl, 200 mM Na₂HPO₄, 50 mM TCEP, 100 mM MPAA, pH 6.8, 25 °C, 2 h. Refolding protocol: Buffer A, 50 mM Tris-HCl, 2 M GND-HCl, 400 mM Arg, 3 mM GSH, 0.9 mM GSSG, pH 8.0, 4 °C, 36 h. Buffer B, 50 mM Tris-HCl, 1 M GND-HCl, 200 mM Arg, 3 mM GSH, 0.9 mM GSSG, pH 8.0, 4 °C, 24 h. Buffer C, 50 mM Tris-HCl, 250 mM NaCl, 100 mM Arg, 3 mM GSH, 0.9 mM GSSG, pH 8.0, 4 °C, 24 h. Buffer D, 50 mM Tris-HCl, 250 mM NaCl, pH 8.0, 4 °C, 12 h. B) HPLC analysis of ligation process and purified RBD 1. C) HRMS of RBD 1. D) HRMS of RBD (2–6). E) CD spectrum of RBDs (1–6). F) SDS-PAGE of expressed peptide II and RBDs (1–6). wt-RBD, wild-type RBD.

7 and 9, providing glycopeptides **19** (67% yield over two steps) and **20** (56% yield over two steps) after TFA deprotection, respectively. It is worth noting that only trace amounts of cyclized byproducts were observed after TFA treatment (see the Supporting Information, page 23 for details).^[19] Importantly, the preparation of glycopeptide fragments **III** and **IV** was readily scaled up, ultimately providing over 10 mg of glycopeptides bearing various defined glycoforms.

With the prerequisite expressed peptide **II** and glycopeptides **III** and **IV** in hand, we proceeded to assemble these peptide segments by NCL to create full sequence RBDs. As an example, peptide hydrazide **13** was activated through the acyl pyrazole activation method developed by Dawson and co-workers,^[20] furnishing thioester **21** at 87% yield after HPLC (Figure 3A). Next, glycopeptide **19** and **21** were ligated under NCL conditions (6 M GND-HCl, 0.1 M Na₂HPO₄, 50 mM TCEP at pH 6.8) with 4-mercaptophenylacetic acid (MPAA) as an additive over 2 h. The RBD (319–360) intermediate **22** containing two *N*-glycans at N331, N 343 was obtained cleanly. Without purification, subsequent in situ activation of peptide hydrazide **22** to peptide thioester yielded **23** at 61% isolated yield over two steps. Despite the difficult Asn-Cys junction, the final projected ligation between ex-

pressed peptide **II** and glycopeptide **23** (containing a C-terminal N360 thioester) was successfully accomplished in an almost quantitative conversion, providing fully glycosylated RBD **24** at 61% isolated yield.

Refolding of the glycosylated RBD presents an arduous challenge due to its structural complexity. It has been reported that many proteins can only be correctly refolded under specified conditions.^[21] After extensive screening of refolding buffer, additives, and dialysis time, we finally refolded RBDs successfully via multistep dialysis (see the Supporting Information, page 45 for details). Glycosylated RBD **1** (0.05 mg mL⁻¹) in a solution of 6 M GND-HCl, 10 mM DTT was denatured at 37 °C for 30 min, then DTT was removed via dialysis against 6 M GND-HCl (pH 8.0, 4 °C, 12 h). The RBD **24** was further dialyzed against refolding buffers (A–D) successively and purified by HPLC, giving RBD **1** at 59% isolated yield. The HPLC shift represents the successful protein refolding process (Figure 3B). High resolution MS, SDS-PAGE, and circular dichroism (CD) spectra further validated the structure of synthetic RBD **1** (Figure 3C, E and F). Enzyme digestion suggests the correct disulfide bonds (Cys336-Cys361, Cys379-Cys432, Cys391-Cys525, and Cys480-Cys488, see the Supporting Information, page 46 for details). Using the same ligation and refolding strategy, five

A ACE2				B S309				C CB6				D AS35			
RBD	k_a (10^5) ($M^{-1}s^{-1}$)	k_d (10^{-3}) (s^{-1})	K_D (nM)	RBD	k_a (10^5) ($M^{-1}s^{-1}$)	k_d (10^{-6}) (s^{-1})	K_D (pM)	RBD	k_a (10^5) ($M^{-1}s^{-1}$)	k_d (10^{-2}) (s^{-1})	K_D (nM)	RBD	k_a (10^5) ($M^{-1}s^{-1}$)	k_d (10^{-3}) (s^{-1})	K_D (nM)
wt	7.60	9.03	11.9	wt	18.2	1.12	0.62	wt	4.43	1.31	29.6	wt	3.16	6.59	20.8
1	5.49	8.70	15.9	1	2.39	878	3680	1	3.87	1.34	32.5	1	3.24	5.78	17.8
2	5.97	7.51	12.6	2	1.57	384	2450	2	4.34	1.30	30.0	2	1.78	4.47	25.0
3	10.1	11.9	11.8	3	3.85	443	1150	3	4.58	1.38	30.2	3	3.85	4.01	17.1
4	7.44	9.25	12.4	4	2.34	154	657	4	4.63	1.42	30.7	4	1.84	6.09	33.1
5	5.50	8.21	14.9	5	1.81	433	2390	5	3.87	1.51	39.1	5	3.38	5.78	26.6
6	5.87	8.29	14.1	6	1.74	644	3690	6	3.59	1.32	36.8	6	1.33	4.67	35.2

Figure 4. Binding kinetics of RBDs to ACE2 and mAbs. A) Synthetic RBDs recognize ACE2 with similar affinity to wt-RBD. B) The binding profile between RBDs and mAb S309. C) The binding profile between RBDs and mAb CB6. D) The binding profile between RBDs and mAb AS35 (ACROBiosystems, anti-SARS-CoV-2 spike RBD neutralizing antibody, Human IgG1, cat. no. SAD-S35). wt-RBD: ACROBiosystems, Arg319-Lys537 with His Tag, cat. no. SPD-C52H1. ACE2: ACROBiosystems, cat. no. AC2-H5257.

RBD surrogates (2–6) bearing different homogeneous glycoforms at N331, N343, and T323 were synthesized in similar yields, and their structures were confirmed by HRMS, CD spectra and SDS-PAGE (Figure 3D, E, and F).

To assess the functions of synthetic RBDs, we next studied the binding of our synthetic RBDs and wild-type RBD (wt-RBD) with ACE2 by surface plasmon resonance (SPR, Biacore). These SPR data indicated that all synthetic RBDs maintained full functionality with wt-RBD (K_D , 11.8 to 15.9 nM, Figure 4A). However, in contrast to our postulation that glycoforms of the RBD might influence ACE2 binding, a direct comparison of their affinities demonstrated that the glycosylation on the RBDs does not impact their binding. To further explore the specific roles of different RBD glycoforms, we measured the binding affinities of these RBDs to anti-SARS-CoV-2 RBD monoclonal antibodies (mAbs) by SPR. Corti, Veesler and co-workers have reported that antibody S309, which has been employed in clinic settings, could target the SARS-CoV-2 RBD with significantly high potency.^[33] The highly conserved N343 glycan with core fucose is one of the major epitopes recognized by S309. The results from SPR suggest that synthetic RBDs bind to S309 with significantly reduced affinity compared to wt-RBD (1000–6000 folds), indicating that a lack of fucose at synthetic RBD N343 decreases the sensitivity of neutralizing antibodies dramatically (Figure 4B). Next, the binding assay of RBDs against mAb CB6,^[34] suggested that CB6 can bind with these RBDs with similar affinities (Figure 4C). Importantly, it also demonstrates that the size of glycans will not influence the binding ability of CB6. The binding assay of RBDs against an mAb AS35 also demonstrates that the size of RBD glycans has slight perturbations on the interaction of RBD with this antibody (Figure 4D). Together, all these data indicate that glycosylation of RBD is unlikely to influence its binding to ACE2, CB6 and AS35. With regard to S309, our experimental results support that S309 utilizes core fucose of N343 to facilitate their interactions. Native glycoforms of N331 and N343 are heavily fucosylated and possess sialylated complex-type glycans.^[4a] At current stage, it is difficult to explore the functions of homogeneous *N*-glycans bearing core fucose and sialic acids. Thus, continue efforts will be employed to prepare fucosylated and sialylated complex-type glycans of RBD in our lab.

Conclusion

The inaugural synthesis of homogeneous glycosylated RBDs, bearing defined structure glycans at N331, N343, and T323, has been achieved through a strategy that is of high convergence and compatible with SARS-CoV-2 RBD library synthesis. The state-of-the-art union of oligo-saccharide, peptide and protein chemistry provides a flexible and robust means to construct structurally defined glycosylated RBDs efficiently. Under selective pressure, the evolution of a virus might result in glycoforms and glycosylation site alteration, and this scalable synthetic platform allows us to prepare homogeneous RBDs efficiently and facilitate the development of effective therapeutics. Further work to evaluate the in vivo immunogenicity of synthetic RBDs is under way. Moreover, the platform represents a versatile strategy for accessing synthetic glycosylated RBDs that could be relevant for other virus studies, including the SAR study of different RBD glycoforms, and verifying the capacity of mAbs for other pathogens such as SARS and MERS. Understanding the specific role of glycosylation on these viral RBDs would pave the way for the future development of effective therapeutics and vaccines.

Acknowledgements

Financial support for this work comes from the National Natural Science Foundation of China (91753102, 22077080, 21907064, 21672146, 21778067, and 21977108), the Interdisciplinary Program of Shanghai Jiao Tong University (YG2020YQ14), the National Key Research Development Program of China (2018YFA0507602), the Key Research Program of Frontier Sciences of the Chinese Academy of Sciences (ZDBS-LY-SLH030), One-hundred Talents Program of Chinese Academy of Sciences and the Shanghai Science and Technology Committee (20S11901100). The authors thank X. Li and Y. Tang (Instrumental Analysis Center, Shanghai Jiao Tong University) for their technical assistance with HRMS and SPR experiments. We thank Prof. Q. Zhang (University at Albany, SUNY), Prof. M. Deng (Huazhong Agricultural University) for helpful discussion and Prof. Yongqiang Tu for analytical equipment access.

Conflict of interest

The authors declare no conflict of interest.

Keywords: glycoproteins · ligation · oligosaccharide · spike

- [1] a) Q. Li, X. Guan, P. Wu, X. Wang, L. Zhou, Y. Tong, R. Ren, K. S. M. Leung, E. H. Y. Lau, J. Y. Wong, X. Xing, N. Xiang, Y. Wu, C. Li, Q. Chen, D. Li, T. Liu, J. Zhao, M. Liu, W. Tu, C. Chen, L. Jin, R. Yang, Q. Wang, S. Zhou, R. Wang, H. Liu, Y. Luo, Y. Liu, G. Shao, H. Li, Z. Tao, Y. Yang, Z. Deng, B. Liu, Z. Ma, Y. Zhang, G. Shi, T. T. Y. Lam, J. T. Wu, G. F. Gao, B. J. Cowling, B. Yang, G. M. Leung, Z. Feng, *N. Engl. J. Med.* **2020**, *382*, 1199–1207; b) C. Huang, Y. Wang, X. Li, L. Ren, J. Zhao, Y. Hu, L. Zhang, G. Fan, J. Xu, X. Gu, Z. Cheng, T. Yu, J. Xia, Y. Wei, W. Wu, X. Xie, W. Yin, H. Li, M. Liu, Y. Xiao, H. Gao, L. Guo, J. Xie, G. Wang, R. Jiang, Z. Gao, Q. Jin, J. Wang, B. Cao, *Lancet* **2020**, *395*, 497–506; c) P. Zhou, X. L. Yang, X. G. Wang, B. Hu, L. Zhang, W. Zhang, H. R. Si, Y. Zhu, B. Li, C. L. Huang, H. D. Chen, J. Chen, Y. Luo, H. Guo, R. D. Jiang, M. Q. Liu, Y. Chen, X. R. Shen, X. Wang, X. S. Zheng, K. Zhao, Q. J. Chen, F. Deng, L. L. Liu, B. Yan, F. X. Zhan, Y. Y. Wang, G. F. Xiao, Z. L. Shi, *Nature* **2020**, *579*, 270–273.
- [2] a) R. Lu, X. Zhao, J. Li, P. Niu, B. Yang, H. Wu, W. Wang, H. Song, B. Huang, N. Zhu, Y. Bi, X. Ma, F. Zhan, L. Wang, T. Hu, H. Zhou, Z. Hu, W. Zhou, L. Zhao, J. Chen, Y. Meng, J. Wang, Y. Lin, J. Yuan, Z. Xie, J. Ma, W. J. Liu, D. Wang, W. Xu, E. C. Holmes, G. F. Gao, G. Wu, W. Chen, W. Shi, W. Tan, *Lancet* **2020**, *395*, 565–574; b) M. Hoffmann, H. Kleine-Weber, S. Schroeder, N. Kruger, T. Herrler, S. Erichsen, T. S. Schiergens, G. Herrler, N. H. Wu, A. Nitsche, M. A. Muller, C. Drosten, S. Pohlmann, *Cell* **2020**, *181*, 271–280; c) R. Yan, Y. Zhang, Y. Li, L. Xia, Y. Guo, Q. Zhou, *Science* **2020**, *367*, 1444–1448; d) J. Shang, G. Ye, K. Shi, Y. Wan, C. Luo, H. Aihara, Q. Geng, A. Auerbach, F. Li, *Nature* **2020**, *581*, 221–224.
- [3] a) Q. Wang, Y. Zhang, L. Wu, S. Niu, C. Song, Z. Zhang, G. Lu, C. Qiao, Y. Hu, K. Y. Yuen, Q. Wang, H. Zhou, J. Yan, J. Qi, *Cell* **2020**, *181*, 894–904; b) D. Wrapp, N. Wang, K. S. Corbet, J. A. Goldsmith, C.-L. Hsieh, O. Abiona, B. S. Graham, J. S. McLellan, *Science* **2020**, *367*, 1260–1263; c) Y. Wu, F. Wang, C. Shen, W. Peng, *Science* **2020**, *368*, 1274–1278; d) R. Shi, C. Shan, X. Duan, Z. Chen, P. Liu, J. Song, T. Song, X. Bi, C. Han, L. Wu, G. Gao, X. Hu, Y. Zhang, Z. Tong, W. Huang, W. J. Liu, G. Wu, B. Zhang, L. Wang, J. Qi, H. Feng, F. S. Wang, Q. Wang, G. F. Gao, Z. Yuan, J. Yan, *Nature* **2020**, *584*, 120–124; e) D. Pinto, Y. J. Park, M. Beltramello, A. C. Walls, M. A. Tortorici, S. Bianchi, S. Jaconi, K. Culap, F. Zatta, A. De Marco, A. Peter, B. Guarino, R. Spreafico, E. Cameroni, J. B. Case, R. E. Chen, C. Havenar-Daughton, G. Snell, A. Telenti, H. W. Virgin, A. Lanzavecchia, M. S. Diamond, K. Fink, D. Vesleser, D. Corti, *Nature* **2020**, *583*, 290–295; f) J. Lan, J. Ge, J. Yu, S. Shan, H. Zhou, S. Fan, Q. Zhang, X. Shi, Q. Wang, L. Zhang, X. Wang, *Nature* **2020**, *581*, 215–220; g) M. Yuan, N. C. Wu, X. Zhu, C.-C. D. Lee, R. T. Y. So, H. Lv, C. K. P. Mok, I. A. Wilson, *Science* **2020**, *368*, 630–633; h) J. Yang, W. Wang, Z. Chen, S. Lu, F. Yang, Z. Bi, L. Bao, F. Mo, X. Li, Y. Huang, W. Hong, Y. Yang, Y. Zhao, F. Ye, S. Lin, W. Deng, H. Chen, H. Lei, Z. Zhang, M. Luo, H. Gao, Y. Zheng, Y. Gong, X. Jiang, Y. Xu, Q. Lv, D. Li, M. Wang, F. Li, S. Wang, G. Wang, P. Yu, Y. Qu, L. Yang, H. Deng, A. Tong, J. Li, Z. Wang, J. Yang, G. Shen, Z. Zhao, Y. Li, J. Luo, H. Liu, W. Yu, M. Yang, J. Xu, J. Wang, H. Li, H. Wang, D. Kuang, P. Lin, Z. Hu, W. Guo, W. Cheng, Y. He, X. Song, C. Chen, Z. Xue, S. Yao, L. Chen, X. Ma, S. Chen, M. Gou, W. Huang, Y. Wang, C. Fan, Z. Tian, M. Shi, F. S. Wang, L. Dai, M. Wu, G. Li, G. Wang, Y. Peng, Z. Qian, C. Huang, J. Y. Lau, Z. Yang, Y. Wei, X. Cen, X. Peng, C. Qin, K. Zhang, G. Lu, X. Wei, *Nature* **2020**, *586*, 572–577.
- [4] a) Y. Watanabe, J. D. Allen, D. Wrapp, J. S. McLellan, M. Crispin, *Science* **2020**, *369*, 330–333; b) S. S. Shivatare, C. H. Wong, *J. Org. Chem.* **2020**, *85*, 15780–15800; c) A. Shajahan, N. T. Supekar, A. S. Gleinich, P. Azadi, *Glycobiology* **2020**, *30*, 981–988; d) P. Zhao, J. L. Praissman, O. C. Grant, Y. Cai, T. Xiao, K. E. Rosenbalm, K. Aoki, B. P. Kellman, R. Bridger, D. H. Barouch, M. A. Brindley, N. E. Lewis, M. Tiemeyer, B. Chen, R. J. Woods, L. Wells, *Cell Host Microbe* **2020**, *28*, 586–601.
- [5] Y. Watanabe, Z. T. Berndsen, J. Raghvani, G. E. Seabright, J. D. Allen, O. G. Pybus, J. S. McLellan, I. A. Wilson, T. A. Bowden, A. B. Ward, M. Crispin, *Nat. Commun.* **2020**, *11*, 2688.
- [6] Q. Li, J. Wu, J. Nie, L. Zhang, H. Hao, S. Liu, C. Zhao, Q. Zhang, H. Liu, L. Nie, H. Qin, M. Wang, Q. Lu, X. Li, Q. Sun, J. Liu, L. Zhang, X. Li, W. Huang, Y. Wang, *Cell* **2020**, *182*, 1284–1294.
- [7] M. P. Lenza, I. Oyenarte, T. Diercks, J. I. Quintana, A. Gimeno, H. Coelho, A. Diniz, F. Peccati, S. Delgado, A. Bosch, M. Valle, O. Millet, N. G. A. Abrescia, A. Palazon, F. Marcelo, G. Jimenez-Oses, J. Jimenez-Barbero, A. Arda, J. Ereno-Orbea, *Angew. Chem. Int. Ed.* **2020**, *59*, 23763–23771; *Angew. Chem.* **2020**, *132*, 23971–23979.
- [8] a) M. Cavallari, P. Stallforth, A. Kalinichenko, D. C. Rathwell, T. M. Gronewold, A. Adibekian, L. Mori, R. Landmann, P. H. Seeberger, G. De Libero, *Nat. Chem. Biol.* **2014**, *10*, 950–956; b) B. Aussedat, Y. Vohra, P. K. Park, A. Fernandez-Tejada, S. M. Alam, S. M. Dennison, F. H. Jaeger, K. Anasti, S. Stewart, J. H. Blinn, H. X. Liao, J. G. Sodroski, B. F. Haynes, S. J. Danishefsky, *J. Am. Chem. Soc.* **2013**, *135*, 13113–13120; c) Z. H. Huang, L. Shi, J. W. Ma, Z. Y. Sun, H. Cai, Y. X. Chen, Y. F. Zhao, Y. M. Li, *J. Am. Chem. Soc.* **2012**, *134*, 8730–8733; d) L. Krasnova, C. H. Wong, *J. Am. Chem. Soc.* **2019**, *141*, 3735–3754.
- [9] P. H. Seeberger, *Acc. Chem. Res.* **2015**, *48*, 1450–1463.
- [10] a) R. E. Thompson, T. W. Muir, *Chem. Rev.* **2020**, *120*, 3051–3126; b) N. Hartrampf, A. Saebi, M. Poskus, Z. P. Gates, A. J. Callahan, A. E. Cowfer, S. Hanna, S. Antilla, C. K. Schissel, A. J. Quartararo, X. Ye, A. J. Mijalis, M. D. Simon, A. Loas, S. Liu, C. Jessen, T. E. Nielsen, B. L. Pentelute, *Science* **2020**, *368*, 980–987; c) H. Yin, M. Zheng, H. Chen, S. Wang, Q. Zhou, Q. Zhang, P. Wang, *J. Am. Chem. Soc.* **2020**, *142*, 14201–14209; d) Y. Tan, H. Wu, T. Wei, X. Li, *J. Am. Chem. Soc.* **2020**, *142*, 20288–20298; e) V. R. Pattabiraman, J. W. Bode, *Nature* **2011**, *480*, 471–479; f) H. Chai, K. Le Mai Hoang, M. D. Vu, K. Pasunooti, C. F. Liu, X. W. Liu, *Angew. Chem. Int. Ed.* **2016**, *55*, 10363–10367; *Angew. Chem.* **2016**, *128*, 10519–10523.
- [11] a) P. Wang, S. Dong, J.-H. Shieh, E. Peguero, R. Hendrickson, M. A. S. Moore, S. J. Danishefsky, *Science* **2013**, *342*, 1357–1360; b) M. Murakami, T. Kiuchi, M. Nishihara, K. Tezuka, R. Okamoto, M. Izumi, Y. Kajihara, *Sci. Adv.* **2016**, *2*, e1500678; c) Y. Maki, R. Okamoto, M. Izumi, Y. Kajihara, *J. Am. Chem. Soc.* **2020**, *142*, 20671–20679; d) C. Bello, S. Wang, L. Meng, K. W. Moremen, C. F. Becker, *Angew. Chem. Int. Ed.* **2015**, *54*, 7711–7715; *Angew. Chem.* **2015**, *127*, 7823–7828; e) N. P. Marotta, Y. H. Lin, Y. E. Lewis, M. R. Ambroso, B. W. Zaro, M. T. Roth, D. B. Arnold, R. Langen, M. R. Pratt, *Nat. Chem.* **2015**, *7*, 913–920; f) C. G. F. Graf, C. Schulz, M. Schmalzlein, C. Heinlein, M. Monnich, L. Perkams, M. Puttner, I. Boos, M. Hessefort, J. N. Lombana Sanchez, M. Weyand, C. Steegborn, B. Breiden, K. Ross, G. Schwarzmann, K. Sandhoff, C. Unverzagt, *Angew. Chem. Int. Ed.* **2017**, *56*, 5252–5257; *Angew. Chem.* **2017**, *129*, 5336–5341; g) C. R. Bertozzi, L. L. Kiessling, *Science* **2001**, *291*, 2357–2364; h) C. Li, L. X. Wang, *Chem. Rev.* **2018**, *118*, 8359–8413; i) G. J. L. Bernardes, B. Castagner, P. H. Seeberger, *ACS Chem. Biol.* **2009**, *4*, 703–713.
- [12] T. W. Muir, D. Sondhi, A. P. A. Cole, *Proc. Natl. Acad. Sci. USA* **1998**, *95*, 6705–6710.
- [13] a) P. Dawson, T. Muir, I. Clark-Lewis, S. Kent, *Science* **1994**, *266*, 776–779; b) S. Bondalapati, M. Jbara, A. Brik, *Nat. Chem.* **2016**,

- 8, 407–418; c) V. Agouridas, O. El Mahdi, V. Diemer, M. Cargoet, J. M. Monbaliu, O. Melnyk, *Chem. Rev.* **2019**, *119*, 7328–7443.
- [14] Based on analysis of the authentic SARS-CoV-2 virus, Li and co-workers reported that the glycoforms of N331 were composed of complex and core structure, see: H. Yao, Y. Song, Y. Chen, N. Wu, J. Xu, C. Sun, J. Zhang, T. Weng, Z. Zhang, Z. Wu, L. Cheng, D. Shi, X. Lu, J. Lei, M. Crispin, Y. Shi, L. Li, S. Li, *Cell* **2020**, *183*, 730–738.
- [15] a) Z.-G. Wang, J. D. Warren, V. Y. Dudkin, X. Zhang, U. Iserloh, M. Visser, M. Eckhardt, P. H. Seeberger, S. J. Danishefsky, *Tetrahedron* **2006**, *62*, 4954–4978; b) V. Ullmann, M. Radisch, I. Boos, J. Freund, C. Pohner, S. Schwarzinger, C. Unverzagt, *Angew. Chem. Int. Ed.* **2012**, *51*, 11566–11570; *Angew. Chem.* **2012**, *124*, 11734–11738.
- [16] G. M. Fang, J. X. Wang, L. Liu, *Angew. Chem. Int. Ed.* **2012**, *51*, 10347–10350; *Angew. Chem.* **2012**, *124*, 10493–10496.
- [17] P. Wang, B. Aussedat, Y. Vohra, S. J. Danishefsky, *Angew. Chem. Int. Ed.* **2012**, *51*, 11571–11575; *Angew. Chem.* **2012**, *124*, 11739–11743.
- [18] X. Liu, J. Liu, Z. Wu, L. Chen, S. Wang, P. Wang, *Chem. Sci.* **2019**, *10*, 8694–8700.
- [19] B. Dang, T. Kubota, K. Mandal, F. Bezanilla, S. B. Kent, *J. Am. Chem. Soc.* **2013**, *135*, 11911–11919.
- [20] D. T. Flood, J. C. J. Hintzen, M. J. Bird, P. A. Cistrone, J. S. Chen, P. E. Dawson, *Angew. Chem. Int. Ed.* **2018**, *57*, 11634–11639; *Angew. Chem.* **2018**, *130*, 11808–11813.
- [21] E. De Bernardez Clark, *Curr. Opin. Biotechnol.* **1998**, *9*, 157–163.

Manuscript received: January 13, 2021

Revised manuscript received: February 23, 2021

Accepted manuscript online: March 11, 2021

Version of record online: April 9, 2021